NACA RM E56G09a

RESEARCH MEMORANDUM

PERFORMANCE OF A DOUBLE-RAMP SIDE INLET WITH COMBINATIONS OF FUSELAGE, RAMP, AND THROAT BOUNDARY-LAYER REMOVAL MACH NUMBER RANGE, 1.5 TO 2.0

By Paul C. Simon

Lewis Flight Propulsion Laboratory
Cleveland, Ohio

NATIONAL ADVISORY COMMITTEE FOR AERONAUTICS
WASHINGTON
October 22, 1956

NACA RM E56G09a

NATIONAL ADVISORY COMMITTEE FOR AERONAUTICS

RESEARCH MEMORANDUM

PERFORMANCE OF A DOUBLE-RAMP SIDE INLET WITH COMBINATIONS OF FUSELAGE, RAMP, AND THROAT BOUNDARY-LAYER REMOVAL MACH NUMBER RANGE, 1.5 TO 2.0

By Paul C. Simon

SUMMARY

The performance of a double-ramp side inlet was investigated with various combinations of fuselage, ramp, and internal throat boundary-layer removal at free-stream Mach numbers of 1.5 to 2.0.

The installation of inlet side fairings produced a 4-percent increase in net propulsive thrust when the inlet was matched to a hypothetical turbojet engine at a Mach number of 2.0. There was, however, a concomitant large reduction in subcritical stability. The side fairings were ineffective at Mach numbers of 1.5 and 1.8.

When a slotted throat bleed and ramp perforations were applied to the inlet, an additional 4-percent increase in net propulsive thrust was realized. No subcritical stability was observed at a Mach number of 2.0.

Increases in net thrust of 4 percent at Mach numbers of 1.5 and 1.8 were realized when the ramp boundary layer was bled through ramp and throat perforations. In addition, inlet stability range and diffuser-exit total-pressure distortions were improved.

In each case investigated it was necessary to divert two-thirds or more of the fuselage boundary layer to obtain maximum inlet performance.

Author

INTRODUCTION

Substantial improvements in side inlet, internal performance are demonstrated, for example, in reference 1 by raising the inlet entirely out of the fuselage boundary layer. Further gains were realized in reference 2 by bleeding off the external-compression-surface boundary-layer

air at the inlet throat. Reference 3 indicates that the stable mass-flow range of an inlet could be extended if external-compression-surface boundary-layer separation was prevented by the application of suction through perforations in the compression surface.

The interrelation of these three methods of boundary-layer control was studied in the NACA Lewis 8- by 6-foot supersonic wind tunnel at free-stream Mach numbers of 1.5 to 2.0. The test configuration consisted of a two-dimensional ramp-type side inlet mounted on a slender body of revolution. Experimental results were recently published in reference 4 for a 14° ramp inlet using a flush-slot throat bleed in combination with a fuselage boundary-layer diverter system. The present study evaluates the optimum net-thrust-minus-configuration-drag and other inlet characteristics for a double-ramp (14° and 8°) inlet with boundary-layer removal through flush slots or ramp perforations or both.

SYMBOLS

$A_{B,e}$ internal-bleed minimum exit area, sq in.

$A_{B,i}$ internal-bleed entrance area (perforations or throat slots or both)

A_f maximum frontal area of basic configuration at $h/\delta = 1$, 0.759 sq ft

A_i inlet capture area, 19.51 sq in.

A_t inlet throat area, 11.85 sq in.

C_D configuration drag coefficient, $D/q_0 A_f$

D configuration drag, lb

D' adjusted configuration drag, lb

D'_b adjusted configuration drag of basic inlet (no internal-bleed system) at $h/\delta = 1$, lb

F internal thrust of turbojet-engine and inlet combination, lb

$F_{n,i}$ ideal net thrust of typical turbojet engine (based on 100-percent pressure recovery), lb

h fuselage boundary-layer diverter height, in.

M Mach number

[redacted]

$\frac{m_2}{m_0}$ main-duct mass-flow ratio, $\frac{\text{main-duct mass flow}}{\rho_0 V_0 A_i}$

P total pressure, lb/sq ft

p static pressure, lb/sq ft

q_0 free-stream dynamic pressure, $\frac{\gamma}{2}\left(p_0 M_0^2\right)$, lb/sq ft

V velocity, ft/sec

w_2 diffuser-exit weight flow per unit flow area, referenced to standard sea-level conditions

$\Delta D'$ incremental adjusted configuration drag, $D_b' - D'$, lb

$\Delta\left(\frac{m_2}{m_0}\right)$ stable mass-flow range, $\left[\left(\frac{m_2}{m_0}\right)_{\text{critical}} - \left(\frac{m_2}{m_0}\right)_{\text{minimum stable}}\right]$

$\Delta P/P_2$ total-pressure distortion at diffuser exit, $\frac{\text{maximum rake total pressure minus minimum rake total pressure}}{\text{area-weighted average total pressure}}$

δ fuselage boundary-layer thickness, approx. 0.55 in.

ρ mass density

γ ratio of specific heats

Subscripts:

b basic inlet configuration: $h/\delta = 1$, no inlet throat-bleed system

0 free-stream conditions

2 diffuser total-pressure survey station, model station 85.0

3 diffuser static-pressure survey station, model station 99.2

APPARATUS AND PROCEDURE

A two-dimensional ramp-type external-compression inlet was mounted beneath a body of revolution consisting of an ogive nose and a 10-inch-diameter cylindrical afterbody downstream of model station 46.2. A

[redacted]

segment of the cylinder was removed to form a flat approach surface to the inlet. This body, the same as the one used in reference 4, is illustrated in figure 1(a). The double ramp used in this test had an initial wedge angle of 14° and a second wedge angle of 22° (angles measured from body axis), as shown in figure 1(b). These angles were selected because the 14° single-ramp inlet of reference 2 gave a high pressure recovery because of a stable second oblique shock, which was generated by boundary-layer separation ahead of the terminal shock and produced an additional 8° flow deflection at a Mach number of 2.0. The present double-ramp compression surface was designed to achieve the advantages of the same two-oblique-shock system of reference 2 without the disadvantages of boundary-layer separation. The positions of the ramps were chosen to place the compression shocks slightly ahead of the inlet cowl lip. Configuration nomenclature, internal-bleed - minimum-exit-area ratio (hereinafter called bleed-area ratio), external diverter height ratios, and pertinent figure numbers of the seven configurations investigated are presented in the following table:

Symbols	Configuration	Bleed-area ratio, $A_{B,i}/A_i$	External diverter height ratio, h/δ	Figure
S	Solid-ramp inlet without side fairings	0	1	4(a)
S_F	Solid-ramp inlet with side fairings	0	1	4(a)
T_F	Throat-bleed inlet with side fairings	.432	1, 2/3, and 0	4(c), (d), and (e)
T	Throat-bleed inlet without side fairings	.432	1	4(f)
$T_{F,P}$	Throat-bleed inlet with side fairings and first ramp perforated	.471	1	4(g)
P_F	Perforated-ramp inlet with side fairings	.464	1, 2/3, and 1/3	4(h), (i), and (j)
P	Perforated-ramp inlet without side fairings	.464	1	4(k)

Detailed drawings of the inlet configurations are shown in figures 1(c), (d), and (e), and photographs of configurations $T_{F,P}$ and P_F are

[redacted]

presented in figures 2(a) and (b), respectively. The inlet side fairings extended from the lip of the cowl sides to the leading edge of the ramp.

4028

The external fuselage boundary-layer system consisted of a 40°-included-angle wedge inserted between the fuselage and the inlet. A range of fuselage boundary-layer diverter heights h of 1, 2/3, 1/3, and 0 times the fuselage boundary-layer thickness δ was available for testing.

The throat boundary-layer removal system consisted of two sharp-cornered flush slots (fig. 2(a)). Air drawn into these slots was ejected through openings in either side of the inlet cowl (see fig. 1(c)).

The variation of the internal-flow area of the diffuser is shown in figure 3. The equivalent cone angle of the over-all diffuser was 4.3°. The rate of diffusion varied with distance and attained a maximum equivalent cone angle of 6° as shown by a comparison of the two curves on figure 3. The model was connected to the support sting by an internal strain-gage balance used to measure axial forces. Inlet mass flow was varied by means of a remotely controlled plug mounted independently of the balance.

Pressure instrumentation consisted of 24 total-pressure tubes and six static-pressure orifices at station 85.0, six static-pressure orifices at station 99.2, nine base-pressure orifices, and two chamber-pressure orifices located in the model balance cavity.

The total-pressure distortion parameter $\Delta P/P_2$ was defined as the maximum diffuser-exit total pressure minus the minimum total pressure divided by the area-weighted average diffuser-exit total pressure. The pitot tubes closest to the diffuser-exit wall were 6.8 percent of the diffuser diameter from the wall surface.

Main-duct mass-flow ratio was determined from the average static pressure at model station 99.2 and the known area ratio between that station and the exit plug where the flow was assumed to be choked. The one-dimensional diffuser-exit total-pressure recovery at model station 85.0 was calculated by an area integration of the measured pressures. The forces resulting from the change in total momentum from free stream to the diffuser exit and all base forces have been excluded from the model force data.

Subcritical flow instability was determined by observing terminal-shock oscillations in the schlieren viewer. Operation of the diffuser in the buzz region was avoided to prevent model damage; however, for all stable points, the amplitude of the static-pressure fluctuations at the diffuser exit was less than 2 percent of free-stream total pressure.

[redacted]

The model was tested at zero angles of attack and yaw and at Mach numbers of 1.5, 1.8, and 2.0. At each external diverter height ratio and Mach number, main-duct mass-flow ratio was varied for several internal-bleed areas. Reynolds number varied from 4×10^6 to 5×10^6 per foot.

The Mach numbers in front of the inlets were experimentally determined to be equal to free-stream Mach numbers.

RESULTS AND DISCUSSION

Inlet Performance

Inlet performance characteristics, consisting of diffuser-exit total-pressure distortion $\Delta P/P_2$, total-pressure recovery P_2/P_0, and external drag coefficient C_D, are presented in figure 4. These data are plotted as a function of main-duct mass-flow ratio m_2/m_0 for several combinations of external and internal boundary-layer removal. Lines of constant weight flow per unit diffuser-exit flow area (referenced to standard sea-level conditions) w_2 are superimposed on the figures for convenience in engine-inlet matching analyses. The solid symbols represent the conditions of minimum stable mass-flow ratio before the onset of buzz. An $\times$ has been placed on each pressure-recovery - mass-flow curve to indicate the point of maximum thrust-minus-incremental-drag ratio as determined from a variable-size inlet matched to a hypothetical turbojet engine at all points on the curve. A more detailed explanation and analysis of these points will be discussed later.

Solid-ramp inlet. - Figure 4(a) shows the effect of side fairings on the performance of the solid-ramp inlet with an external diverter height ratio h/δ of 1. The only significant change with the addition of side fairings was a 5-percent increase in critical mass flow with a concomitant 79-percent reduction in stable mass-flow range at a Mach number of 2.0.

Critical, subcritical, and minimum stable shock patterns for the inlet without side fairings at a Mach number of 2.0 are shown in the schlieren photographs of figure 4(b). The second oblique shock for the critical case fell inside the cowl lip. The peak recovery condition reveals that the slip line, emanating from the intersection of the first oblique and the terminal shocks, has entered the inlet without causing buzz. This also occurred for the case with side fairings. The minimum stable shock pattern just prior to the onset of buzz is also shown.

Throat-bleed inlet. - The performance of the throat-bleed inlet with side fairings (configuration T_F) is presented in figures 4(c), (d), and (e) for external diverter height ratios of 1, 2/3, and 0, respectively, and various bleed-area ratios.

The variation in pressure recovery with mass-flow ratio of configuration S is superimposed on the data of figures 4(c) to (k) for reference. With the throat-bleed exit doors closed ($A_{B,e}/A_t = 0$) at a Mach number of 2.0 and an h/δ of 1, the inlet stability range, critical pressure recovery, and total-pressure distortions indicated a slight improvement over configuration S_F (solid-ramp inlet with side fairings). However, at all Mach numbers and external boundary-layer diverter heights, when the bleed doors were opened, peak pressure recovery increased and total-pressure distortions decreased with a concomitant increase in configuration drag coefficient and decreases in mass-flow ratio and stable mass-flow range. Improvement in recovery and distortion is the result of the ability of the throat-bleed system to remove the separated ramp boundary-layer air caused by the terminal-shock - boundary-layer interaction. The increase in critical drag coefficient is due to the increase in quantity and method of spilling mass flow. Reduction in stable mass-flow range is typical of inlets incorporating throat bleed; however, the reason is not understood.

At a Mach number of 2.0 and an h/δ of 1 (fig. 4(c)), the maximum pressure recovery occurred at a bleed-area ratio $A_{B,e}/A_t$ of 0.20. It was estimated from the difference in critical diffuser mass-flow ratio between configurations S_F and T_F that, at a bleed-area ratio of 0.20, 4 percent of the critical inlet mass flow was diverted through the throat-bleed system during critical inlet operation. It is impossible to estimate the bleed flow during subcritical operation, since spillage occurs around the cowl lip at this condition. At external diverter height ratios of 1 and 2/3, bleed-area ratios of between 0.10 and 0.20 produced near maximum recoveries at all Mach numbers. However, at an h/δ of 0 (fig. 4(e)) the amount of bleed necessary to obtain the maximum possible recovery was not established; the largest bleed area (35 percent) gave the highest recovery. This higher rate of throat bleed was required, since all the fuselage boundary layer approaching the ramp entered the inlet. Total-pressure recoveries were well below those of configuration S ($h/\delta = 1$) at all free-stream Mach numbers.

The removal of side fairings from the throat-bleed inlet at an h/δ of 1 resulted in a slight decrease in recovery and mass flow and an increase in the stability range. These data are presented in figure 4(f) for Mach numbers of 1.8 and 2.0.

Figure 4(g) presents the performance of the throat-bleed inlet with side fairings and first ramp perforated at an h/δ of 1 for various

[redacted]

bleed-area ratios. Reference 3 shows that the stability range of an axisymmetric two-cone nose inlet could be increased markedly by applying suction through the latter portion of the first-cone surface. The buzz was initiated by the separation incurred when the bow shock interacted with the first-cone boundary layer. Since this case appeared similar to the double ramp discussed herein, perforations were installed and the boundary-layer air, which was drawn off the first ramp, was directed downstream by means of reverse scoops shown in figures 1(d) and 2(a). (A baffle separated the ramp bleed air from the throat bleed air.) Except for about a 5-percent increase in critical mass-flow ratio, all inlet performance parameters at all Mach numbers were virtually unaffected by the addition of perforations.

Perforated-ramp inlet. - Perforations were installed along the entire ramp area, including the throat-bleed area of the previous configurations (see figs. 1(e) and 2(b)). The performance of configuration P_F (the perforated-ramp inlet with side fairings) is presented in figures 4(h), (i), and (j) for external diverter height ratios of 1, 2/3, and 1/3.

Inlet stability was greatly improved at an h/δ of 1 by the addition of perforations on the ramp and inlet throat when the bleed-exit doors were closed. This was accomplished, however, at the expense of distortion, mass flow, and pressure recovery. The improved stability probably occurred because the high pressure behind the terminal shock forced air out of the perforations ahead of the shock. The air exhaust from the ramp perforations probably fixed the position of the boundary-layer-flow separation. Reverse flow persisted when the bleed doors were opened. Configuration P_F offered no substantial improvement in inlet stability range over configuration S at an h/δ of 1. There was, however, about a 2- to 4-percent increase in total-pressure recovery in the Mach number range investigated, when the bleed-area ratio was set at 0.35. The diffuser mass flow and total-pressure distortions were about the same as for configuration S; however, the drag coefficient did rise at a Mach number of 2.0 from a critical value of 0.14 to 0.15. The primary effect of reducing the h/δ of the perforated-ramp inlet was the reduction in critical mass flow at Mach numbers of 1.8 and 2.0, as indicated in figures 4(h), (i), and (j). At a Mach number of 1.5 and an h/δ of 2/3, the stable mass-flow range was increased from 20 percent of critical mass flow for configuration S to 35 percent (fig. 4(i)).

The performance characteristics of configuration P (perforated-ramp inlet without side fairings) are presented in figure 4(k). Comparison of the data with configuration S indicates that slight improvement in peak recovery and stable mass-flow range can be realized at all Mach numbers. However, with ramp bleed of about 5 percent, the critical mass-flow ratio was reduced from 0.88 to 0.83 at a Mach number of 2.0.

[redacted]

Schlieren photographs of configuration P for inlet conditions of approximately critical and subcritical mass flow are shown in figure 4(l) at a Mach number of 2.0. Oblique shocks, emanating from the perforations, can be seen for the condition of approximately critical mass flow. Boundary-layer-flow separation occurred subcritically, and an enlarged view of the ramp surface for the subcritical condition reveals air issuing outward from the ramp perforations. This may be the result of high bleed-chamber pressure originating at the throat perforations, which are subjected to high static pressure behind the terminal shock. A method of maintaining positive suction to the perforations probably would have extended the stable mass-flow range.

Propulsive Thrust

The effect of internal throat bleed and external diverter height on the net-thrust-minus-incremental-drag ratio $(F - \Delta D')/F_b$ of the throat-bleed inlet configuration is presented in figure 5(a). This thrust parameter represents the variance in optimum thrust-minus-drag from that of the basic no-bleed configuration (configuration S, fig. 4(a)). The thrust ratios were either optimum thrust ratio or maximum thrust ratio, if sufficient bleed was not obtained to determine the optimum. The thrusts were calculated for a typical turbojet engine assumed to be operating at an altitude of 35,000 feet with maximum afterburner, and at each Mach number the inlet and engine were matched over the mass-flow range for each configuration and each test condition. External drag coefficients were assumed to remain constant while drag was varied in proportion to the changes in inlet size that would be required to accommodate the engine weight flow. The optimum ideal net-thrust-minus-drag ratios $(F - D')/F_{n,i}$ for the solid-ramp inlet without side fairings were 0.52, 0.53, and 0.54 at Mach numbers of 1.5, 1.8, and 2.0, respectively.

The net thrust of the configurations with internal throat bleed at each Mach number tested reached values greater than the basic configuration at diverter height ratios of 2/3 and 1 (fig. 5(a)). At an h/δ of zero, the $(F - \Delta D')/F_b$ remained well below 1 throughout the range of bleed-door settings.

Thus, it can be concluded that, from a net-thrust viewpoint, an h/δ of about 1 is the most desirable. (Ref. 4 states that optimum thrust can be maintained at an h/δ less than 1.) It is interesting to note that at a Mach number of 2.0 and an h/δ of 1 (fig. 5(a)), a gain in thrust of 6 percent was obtained by adding side fairings and throat slots to configuration S, even when the bleed doors were closed. Of this increase, 4 percent can be credited to the side fairings alone.

The greatest gain in $(F - \Delta D')/F_b$ occurred at a Mach number of 2.0 where configuration $T_{F,P}$ reach a value of 8 percent above that obtained for configuration S.

Figure 5(b) shows the net-thrust-minus-incremental-drag ratios for the perforated-ramp inlets at the three Mach numbers investigated for various bleed-area ratios and external diverter height ratios. Gains in the net-thrust parameter up to 4 percent were realized at Mach numbers of 1.5 and 1.8, while at a Mach number of 2.0 the net-thrust ratio was about 10 percent lower than the basic configuration at a bleed-area ratio of zero and increased to a maximum value of 1.0 at maximum bleed-door opening. The net-thrust ratio of the perforated-ramp inlet with side fairings was, in general, several percent higher than that of the perforated-ramp inlet without fairings. Configuration P_F was approximately independent of h/δ (fig. 5(b)) down to an h/δ value of 1/3. At no condition did the net-thrust ratio of configuration P_F with the bleed-exit doors closed equal the net-thrust ratio with bleed.

A bar graph is presented in figure 6 of the maximum net-thrust-minus-incremental-drag ratio and the corresponding inlet performance of all the inlet configurations tested. The highest value of $(F - \Delta D')/F_b$ was selected from those inlets which were tested at three different external diverter height ratios. The stable mass-flow range $\Delta(m_2/m_0)$ was taken as the difference in mass-flow ratio between critical mass flow and minimum stable mass flow. Configuration drag ratio $D'/F_{n,i}$ is the ratio of the configuration drag (adjusted for changes in maximum frontal area to accommodate the engine weight flow) to the ideal net thrust of the typical jet engine at the appropriate free-stream Mach number.

The throat-bleed inlets with side fairings produced gains in net-thrust ratio from 2 to 8 percent over the basic solid-ramp inlet at all three Mach numbers investigated. The largest gain was obtained with configuration $T_{F,P}$ at a Mach number of 2.0, where the net-thrust ratio was 1.08. This improvement was a direct result of increases in mass flow and pressure recovery with a concomitant drop in adjusted configuration drag. Configuration $T_{F,P}$ had no stable mass-flow range and the inlet side fairings prevented the use of the schlieren system to ascertain the point of boundary-layer separation. Total-pressure distortions for all throat-bleed inlets were about 10 percent at all Mach numbers.

The perforated-ramp inlets were the only configurations tested that showed improvements in both thrust and stable mass-flow range. This occurred at a Mach number of 1.5 and possibly at a Mach number of 1.8. At a Mach number of 2.0, the thrust ratio was equal to or less than configuration S because of the reduction in mass flow. Diffuser total-pressure distortions were improved at all Mach numbers.

[redacted]

The performance of the configuration having the highest net-thrust-minus-incremental-drag of reference 4 was selected for comparison and is included in figure 6. This inlet had a 14° ramp angle, a 19° external cowl angle, and a single flush slot in the throat. Throat and fuselage boundary-layer control was varied in the same manner as for the configurations in this report.

Thrust ratios of 15 percent at Mach numbers of 1.5 and 1.8 and 9 percent at a Mach number of 2.0 greater than configuration S are indicated. These peak values were obtained at external diverter height ratios of 1/3, 2/3, and 1 at Mach numbers of 1.5, 1.8, and 2.0, respectively. The lower $D'/F_{n,i}$ of the 14° ramp inlet accounts for the high $(F-\Delta D')/F_b$ values at Mach numbers of 1.5 and 2.0. Although distortions were in the order of 10 percent, the stable mass-flow range was under 0.18 at all Mach numbers.

SUMMARY OF RESULTS

The performance of a double-ramp side inlet with variations in internal and external boundary-layer removal was evaluated in the Lewis 8- by 6-foot supersonic wind tunnel at Mach numbers of 1.5, 1.8, and 2.0. The following results were obtained:

1. The installation of inlet side fairings produced a 4-percent increase in net propulsive thrust when the inlet was matched to a hypothetical turbojet engine at a Mach number of 2.0. The stable mass-flow range, however, was considerably reduced. Side fairings were ineffective at Mach numbers of 1.5 and 1.8.

2. The application of throat bleed, ramp perforations, and side fairings to the double-ramp inlet produced gains in thrust-minus-incremental-drag of between 2 and 8 percent at Mach numbers from 1.5 to 2.0. At a Mach number of 2.0, however, the stable inlet mass-flow range was reduced to zero.

3. The installation of perforations on the ramp and throat surface caused reverse flow in the bleed chamber under the ramp during subcritical operation. Gains of 4 percent in thrust-minus-incremental-drag were obtained at Mach numbers of 1.5 and 1.8 with some improvement in stable mass-flow range. Perforations were ineffective at a Mach number of 2.0.

4. Diffuser total-pressure distortions were reduced from about 20 to 10 percent of the average diffuser total pressure by the use of all types of ramp boundary-layer control tested.

[redacted]

5. Maximum inlet performance occurred with an external boundary-layer diverter height to fuselage boundary-layer thickness ratio of between 2/3 and 1.

Lewis Flight Propulsion Laboratory
National Advisory Committee for Aeronautics
Cleveland, Ohio, July 25, 1956

REFERENCES

1. Weinstein, M. I.: Performance of Supersonic Scoop Inlets. NACA RM E52A22, 1952.

2. Campbell, Robert C.: Performance of a Supersonic Ramp Inlet with Internal Boundary-Layer Scoop. NACA RM E54I01, 1954.

3. Connors, James F., and Meyer, Rudolph C.: Performance Characteristics of Axisymmetric Two-Cone and Isentropic Nose Inlet at Mach Number 1.90. NACA RM E55F29, 1955.

4. Campbell, Robert C.: Performance of Supersonic Ramp-Type Side Inlet with Combinations of Fuselage and Inlet Throat Boundary-Layer Removal. NACA RM E56A17, 1956.

[redacted]

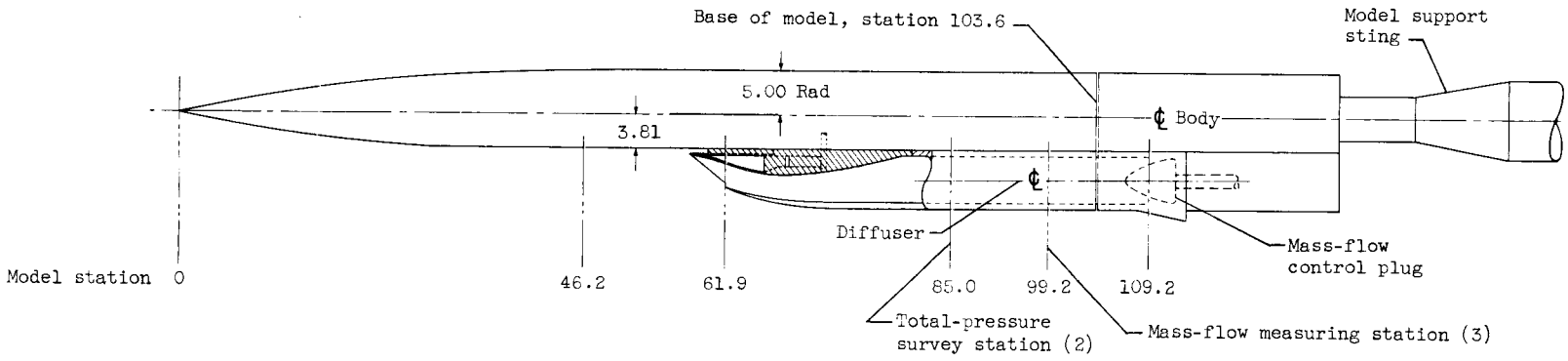

(a) Side view.

x	y	z	w
0	1.25	3.75	3.78
2.00	1.98	4.42	4.63
4.00	2.40	4.88	5.27
6.00	2.54	5.17	5.67
8.00	2.43	5.33	5.83
10.00	2.17	5.41	5.91
12.00	1.83	5.44	5.94
14.00	1.45	↓	↓
16.00	1.03		
18.00	0.53		
20.00	0.00		

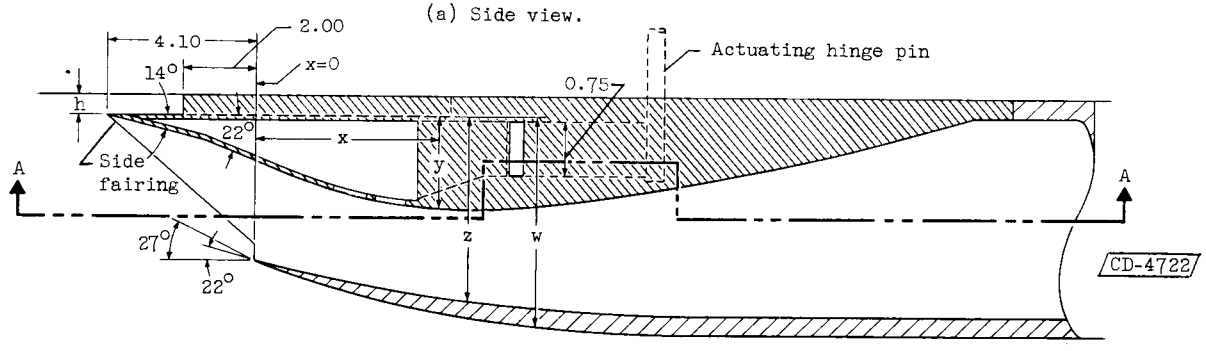

(b) Enlarged cross-sectional side view of inlet.

Figure 1. - Schematic drawings of model and inlet. (All dimensions in inches except where noted.)

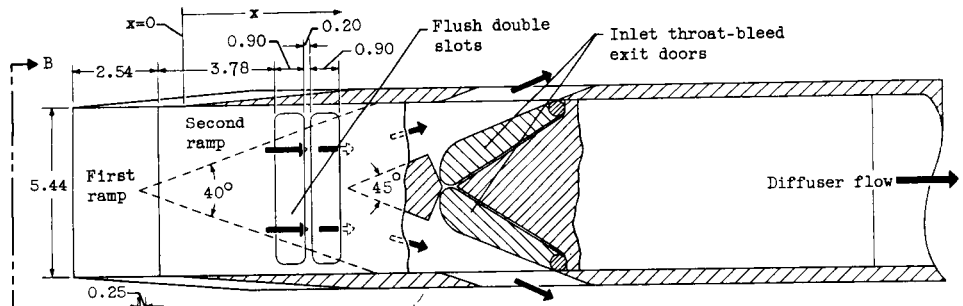

(c) Configuration T_F (throat-bleed inlet with side fairings).

x	R_1	R_2
0	8.75	0.62
2.00	8.48	
4.00	8.23	
6.00	7.97	
8.00	7.71	
10.00	7.44	
12.00	7.18	
14.00	6.62	0.87
16.00	5.71	1.34
18.00	4.41	1.96
20.00	2.72	2.72

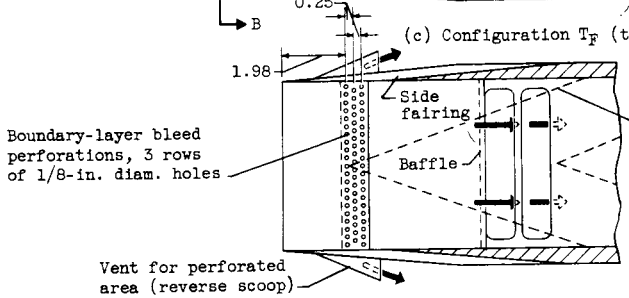

(d) Configuration $T_{F,P}$ (throat-bleed inlet with side fairings and first ramp perforated).

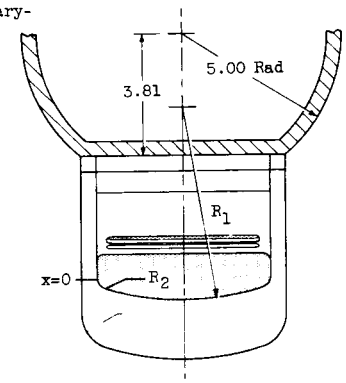

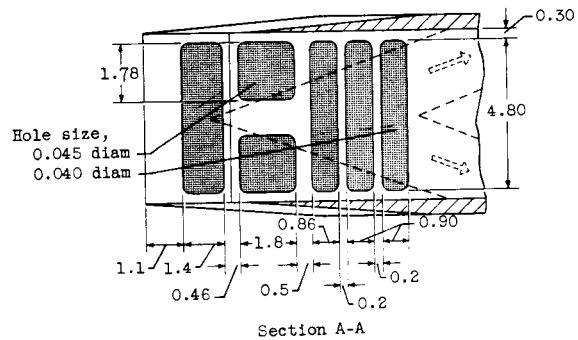

(e) Configuration P_F (perforated-ramp inlet with side fairings).

Figure 1. - Concluded. Schematic drawings of model and inlet. (All dimensions in inches except where noted).

CD-5007

(a) Configuration $T_{F,P}$ (throat-bleed inlet with side fairings and first ramp perforated). Perforated area, 0.75 square inch; slotted throat area, 8.43 square inches.

Figure 2. - Inlet configurations.

(b) Configuration P_F (perforated-ramp inlet). Perforated area, 9.06 square inches.

Figure 2. - Concluded. Inlet configurations.

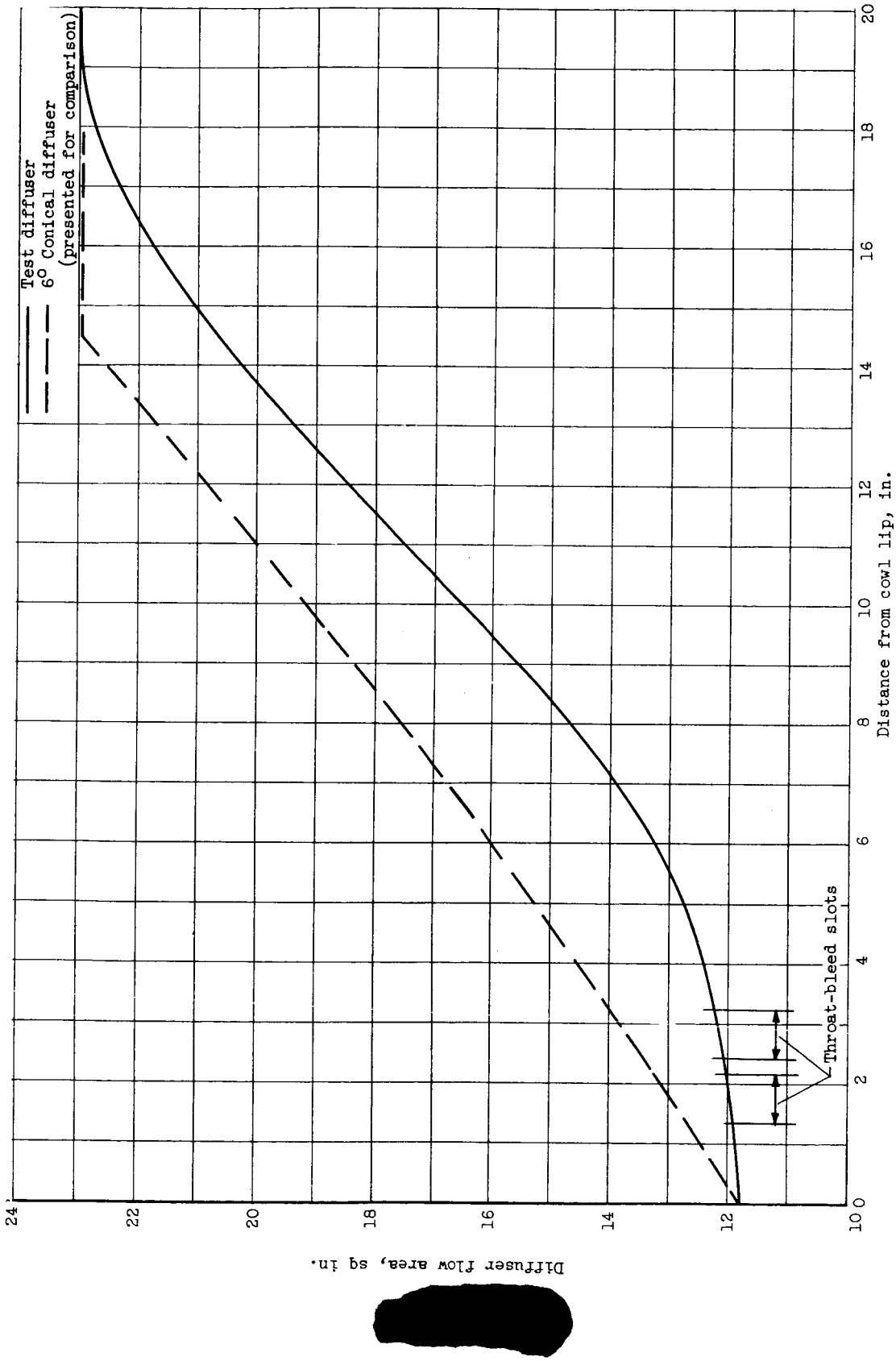

Figure 3. - Diffuser internal-flow area variation. Exit area at model station 85.0, 22.96 square inches.

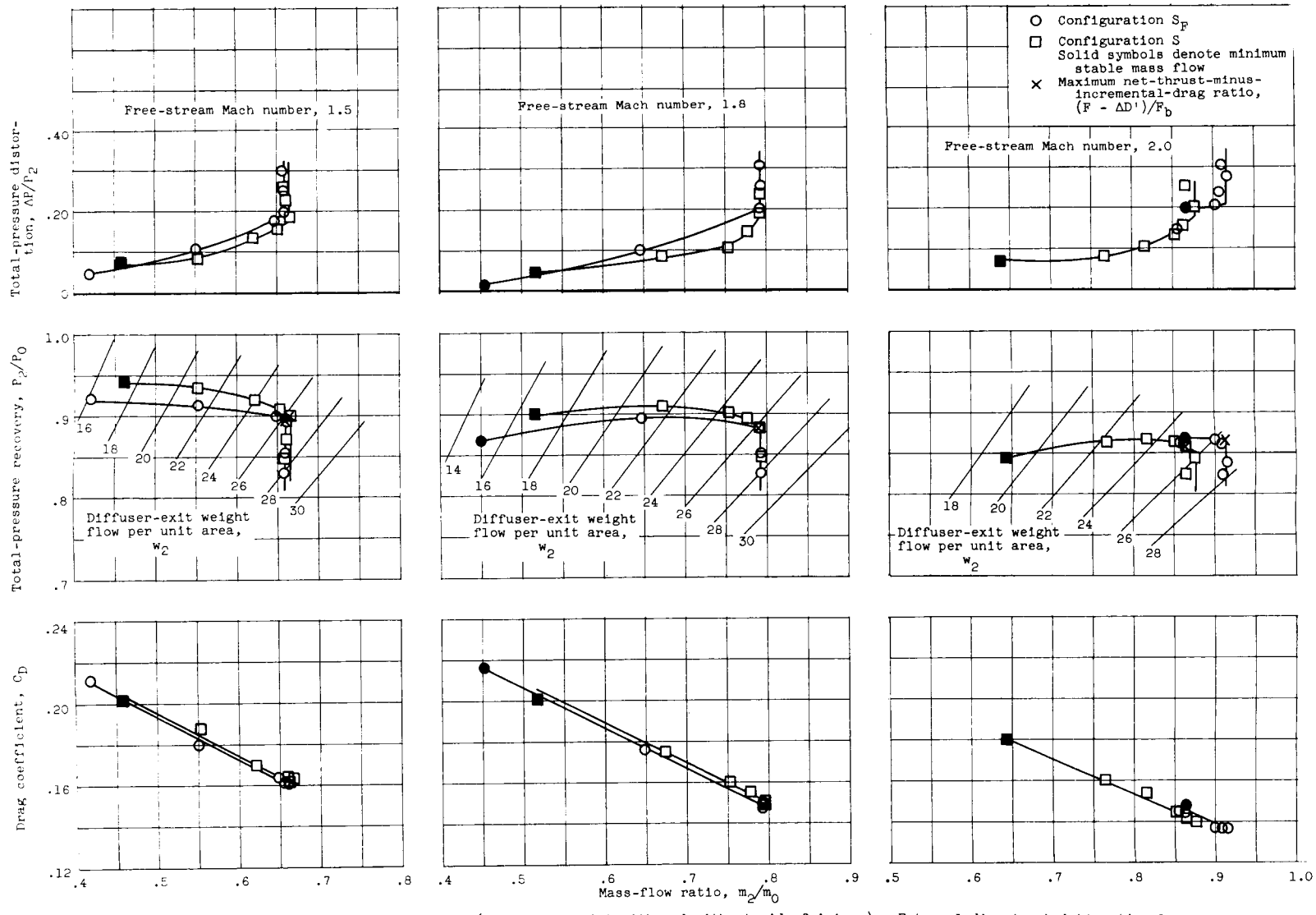

(a) Configurations S_F and S (solid-ramp inlet with and without side fairings). External diverter height ratio, 1.

Figure 4. - Performance characteristics of inlet configurations.

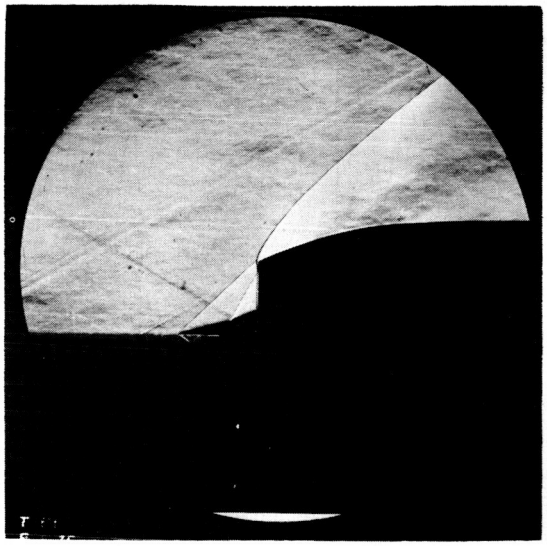

Critical; mass-flow ratio, 0.88; total-pressure recovery, 0.84.

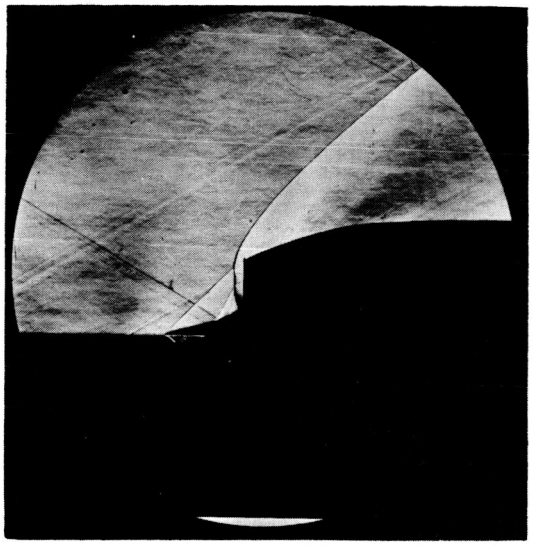

Subcritical (peak recovery); mass-flow ratio, 0.82; total-pressure recovery, 0.87

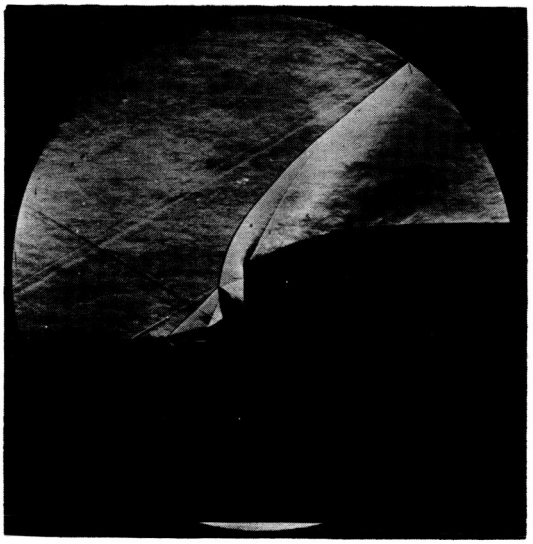

Subcritical (minimum stable); mass-flow ratio, 0.64; total-pressure recovery, 0.84

C-42600

(b) Schlieren photographs of configuration S (solid-ramp inlet without side fairings) at Mach number of 2.0. External diverter height ratio, 1.

Figure 4. - Continued. Performance characteristics of inlet configurations.

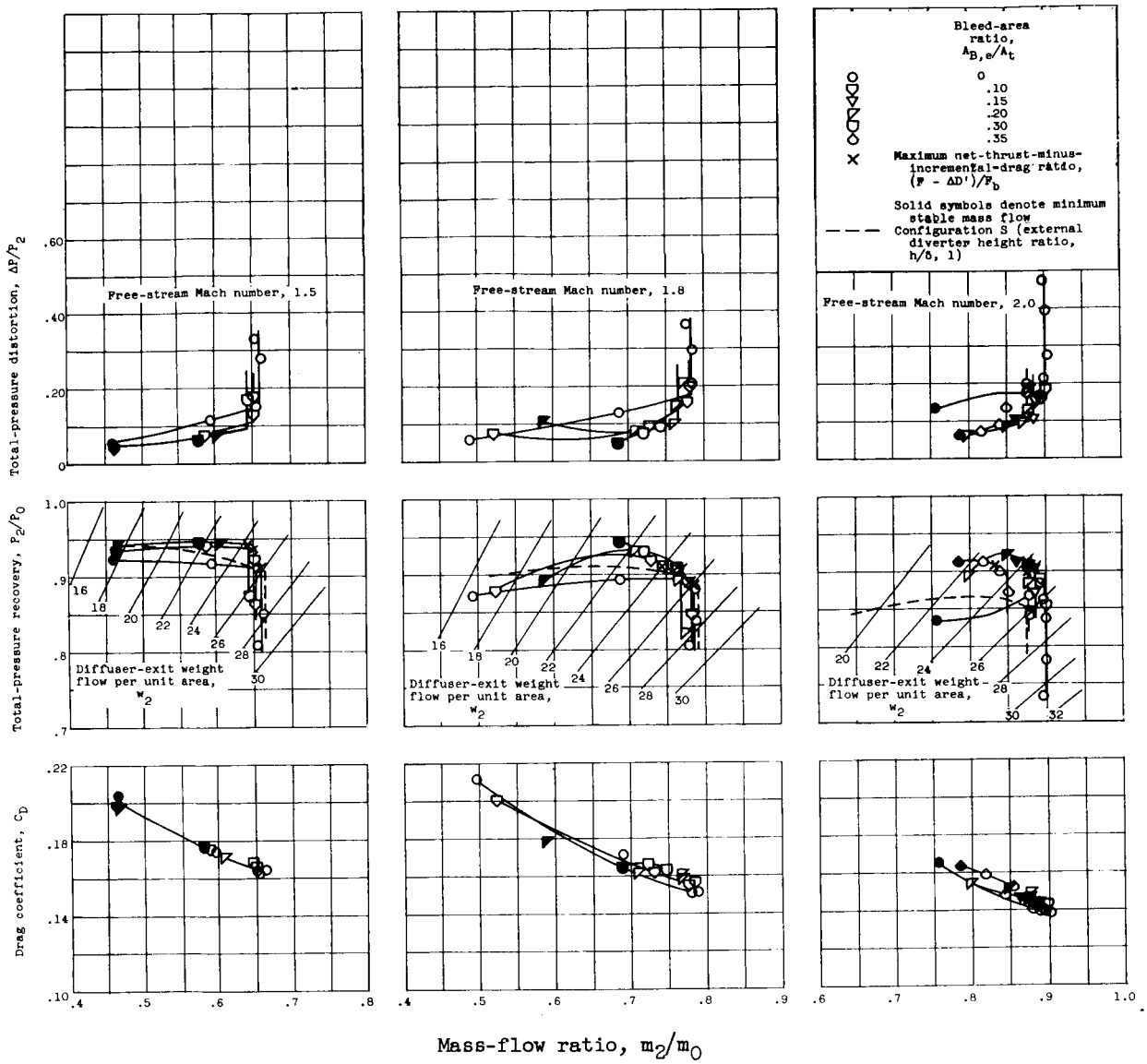

(c) Configuration T_F (throat-bleed inlet with side fairings). External diverter height ratio, 1.

Figure 4. - Continued. Performance characteristics of inlet configurations.

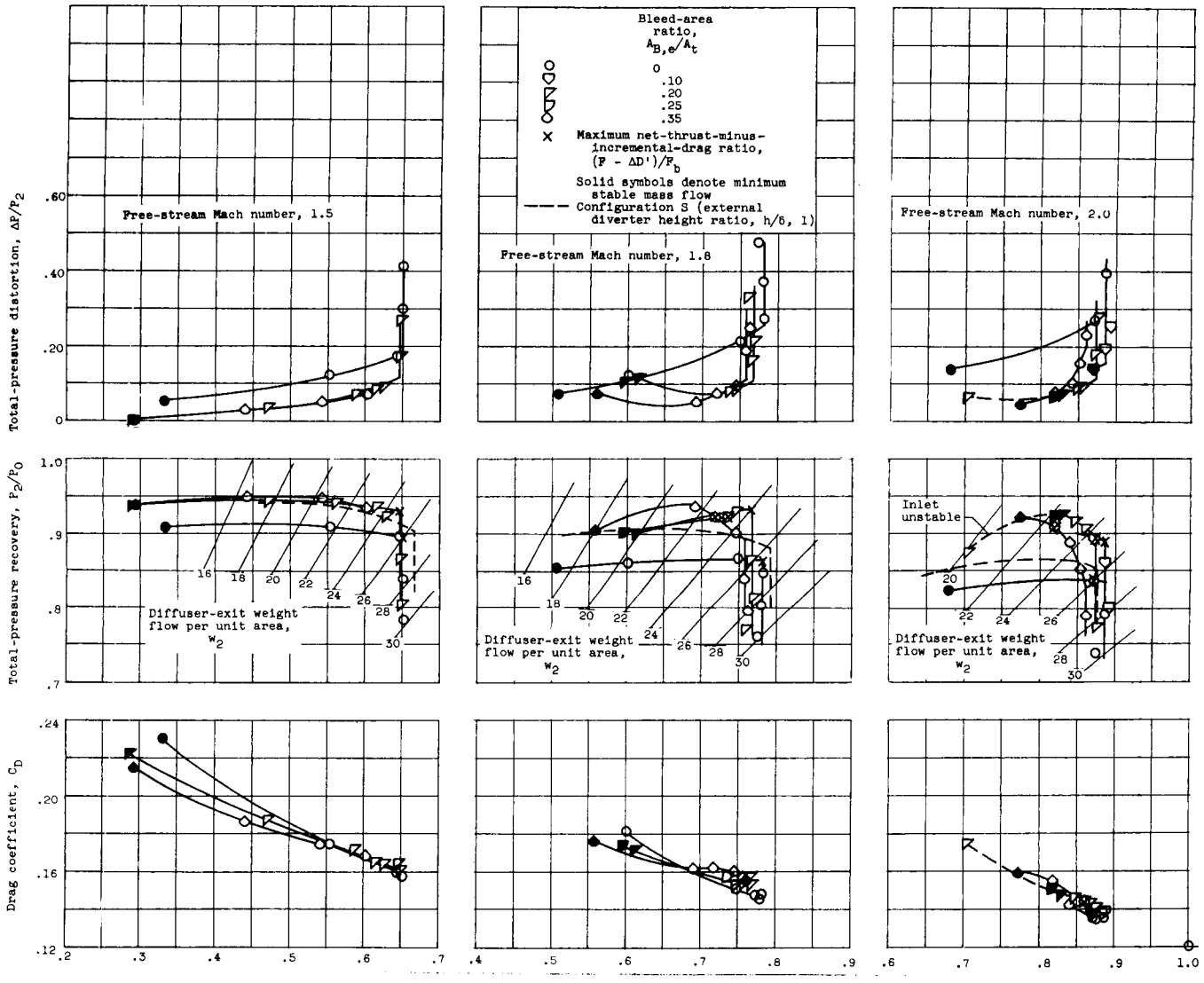

(d) Configuration T_F (throat-bleed inlet with side fairings). External diverter height ratio, 2/3.

Figure 4. - Continued. Performance characteristics of inlet configurations.

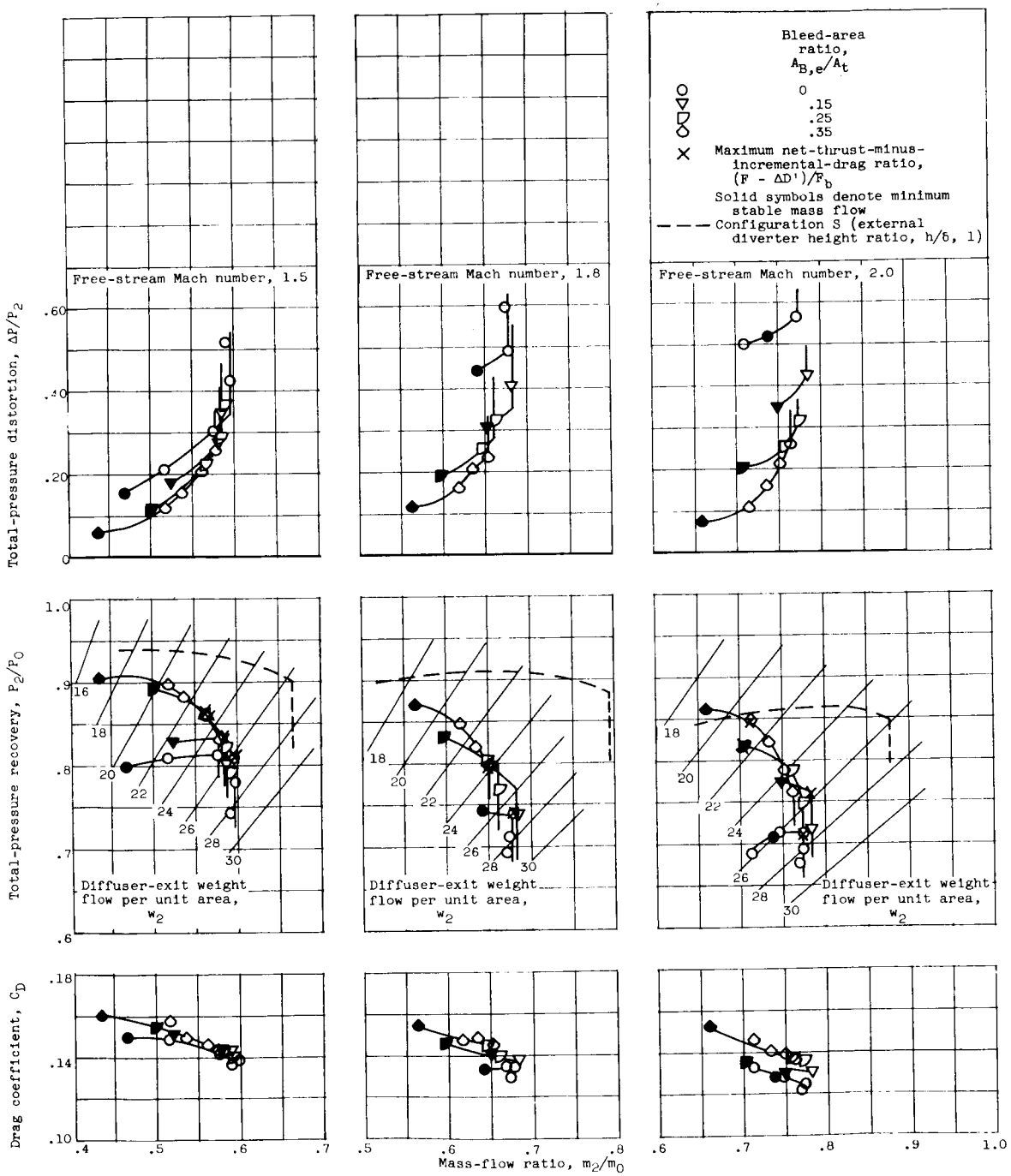

(e) Configuration T_F (throat-bleed inlet with side fairings). External diverter height ratio, 0.

Figure 4. - Continued. Performance characteristics of inlet configurations.

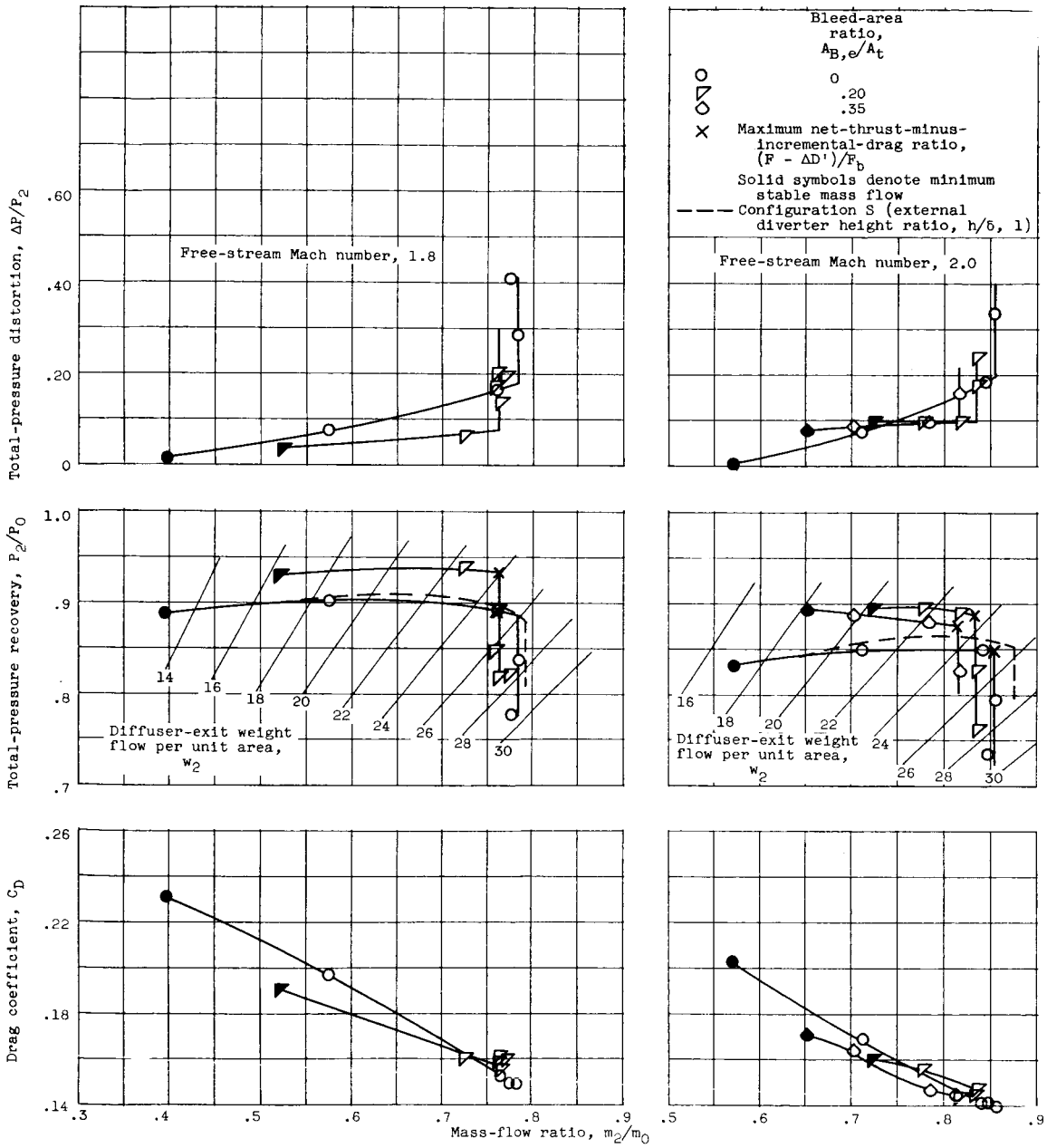

(f) Configuration T (throat-bleed inlet without side fairings). External diverter height ratio, 1.

Figure 4. - Continued. Performance characteristics of inlet configurations.

[redacted]

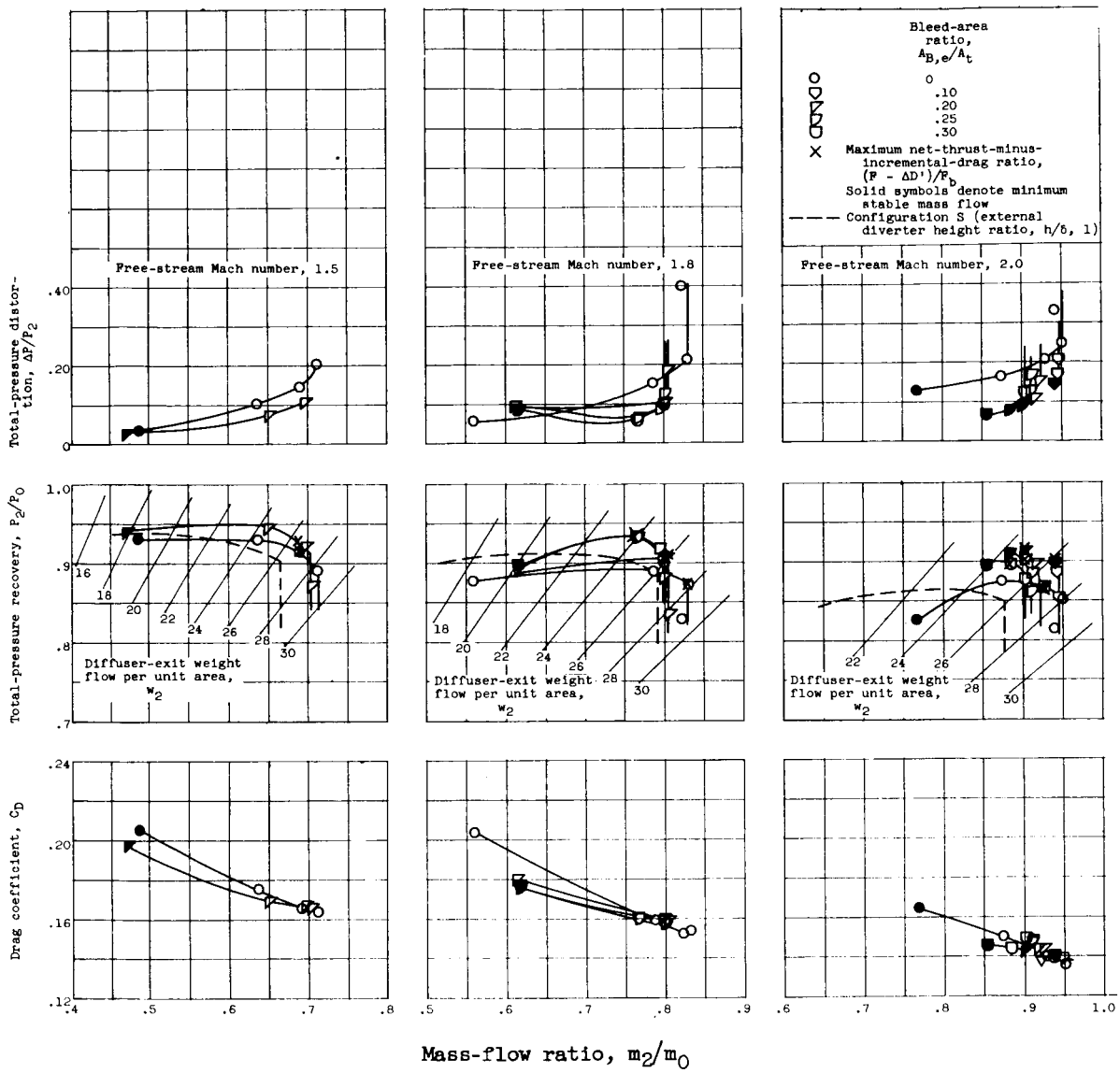

(g) Configuration $T_{F,P}$ (throat-bleed inlet with side fairings and first ramp perforated). External diverter height ratio, 1.

Figure 4. - Continued. Performance characteristics of inlet configurations.

[redacted]

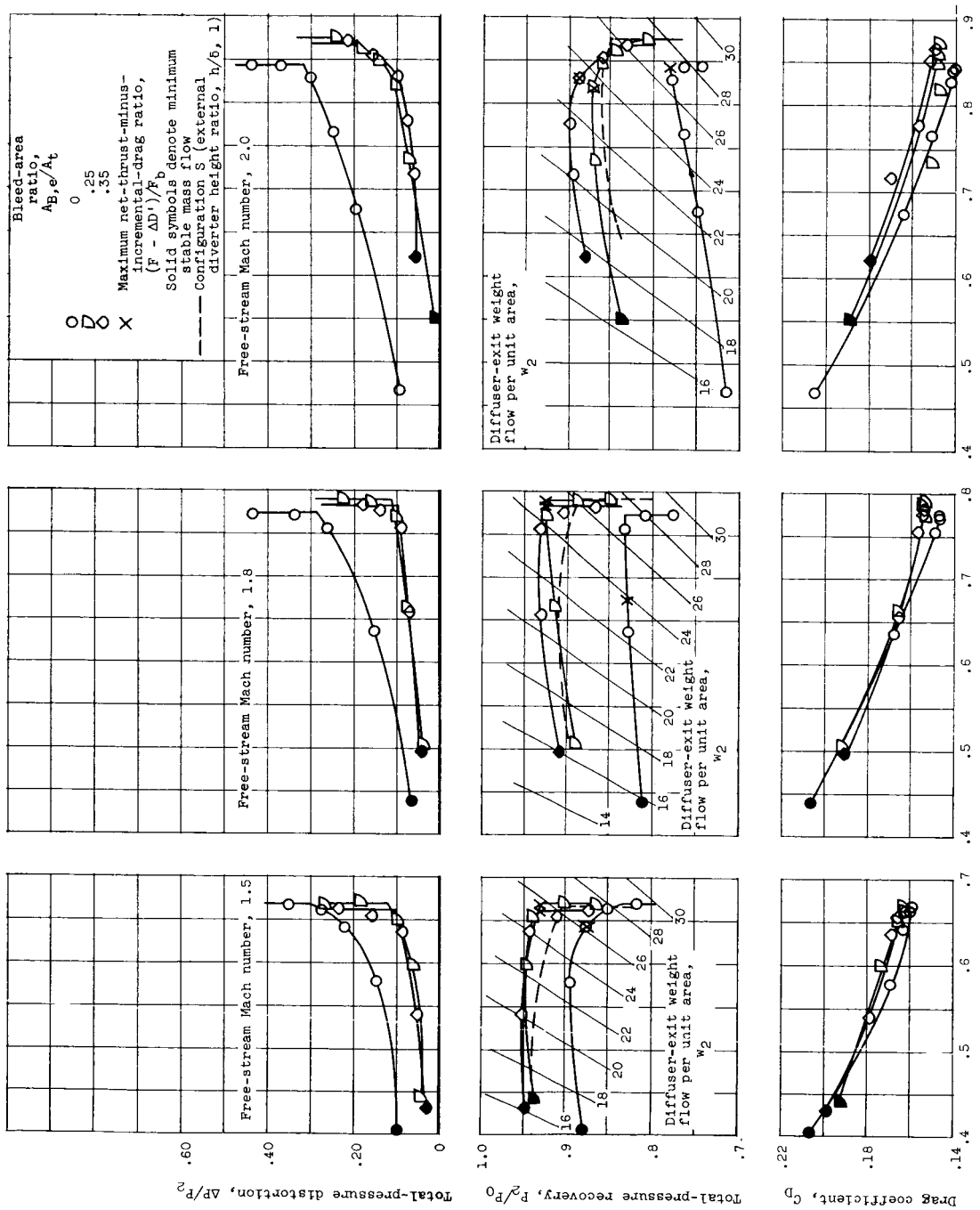

(h) Configuration P_F (perforated-ramp inlet with side fairings). External diverter height ratio, 1.

Figure 4. - Continued. Performance characteristics of inlet configurations.

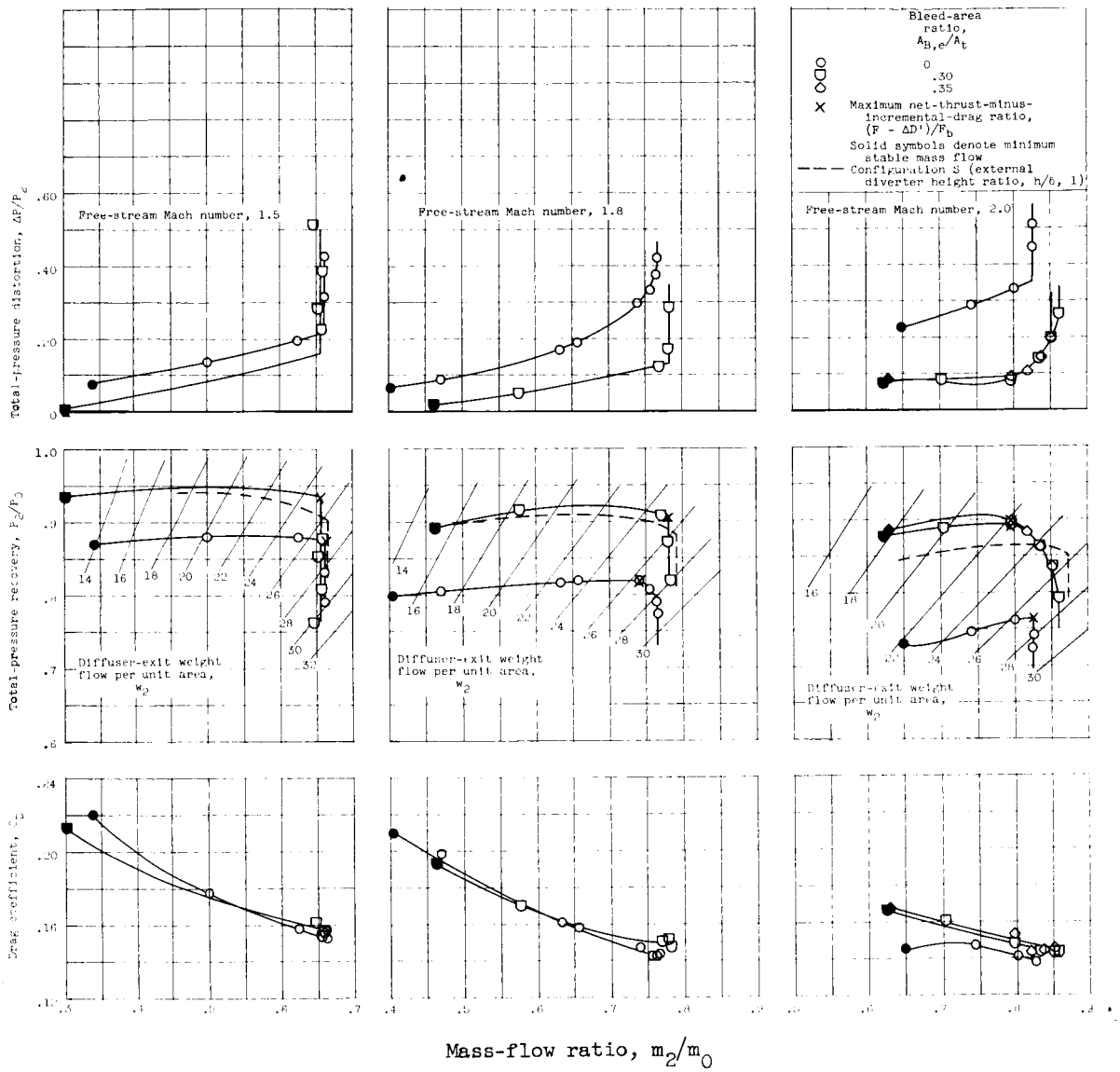

(i) Configuration P_F (perforated-ramp inlet with side fairings). External diverter height ratio, 2/3.

Figure 4. - Continued. Performance characteristics of inlet configurations.

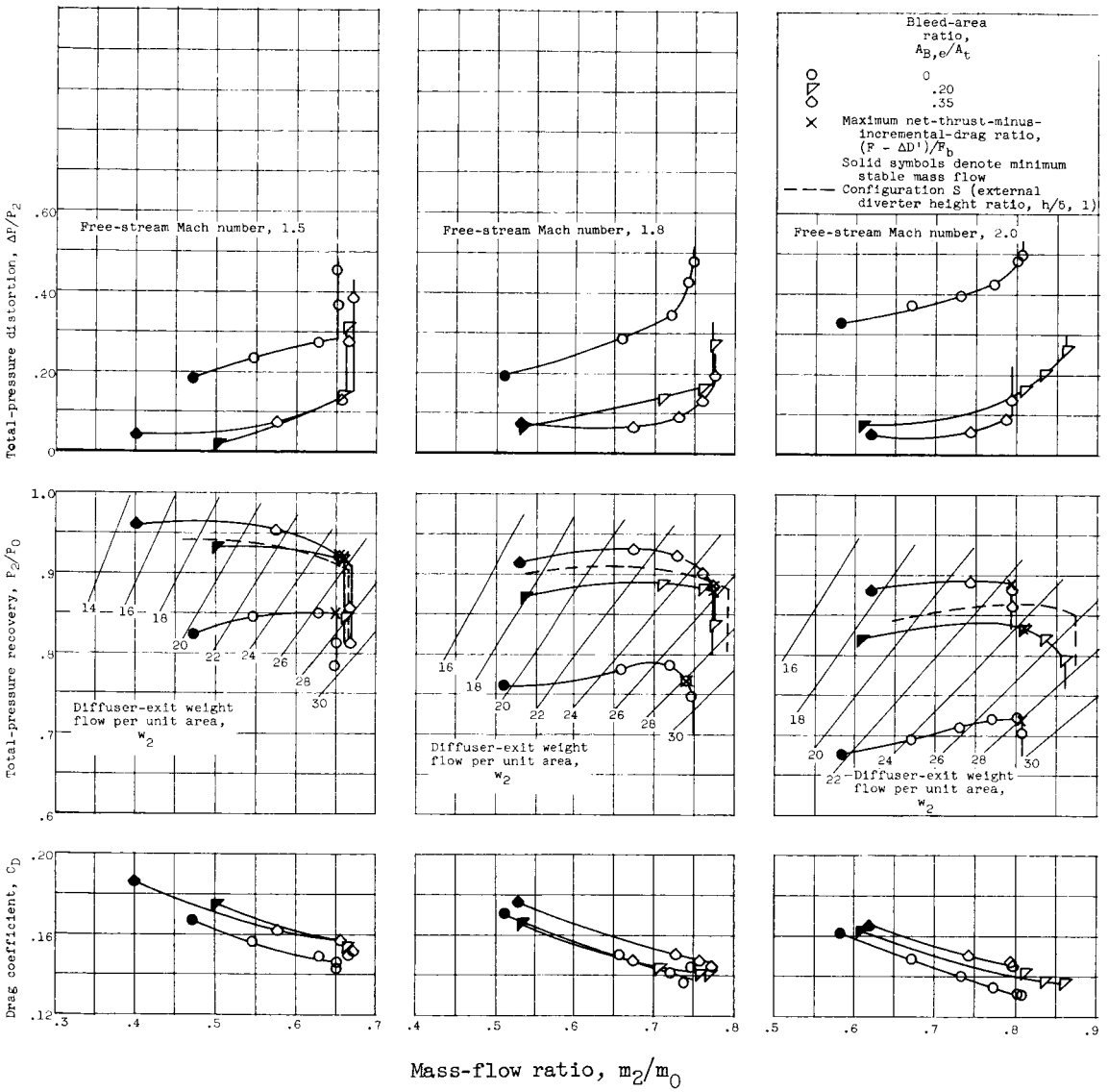

(j) Configuration P_F (perforated-ramp inlet with side fairings). External diverter height ratio, 1/3.

Figure 4. - Continued. Performance characteristics of inlet configurations.

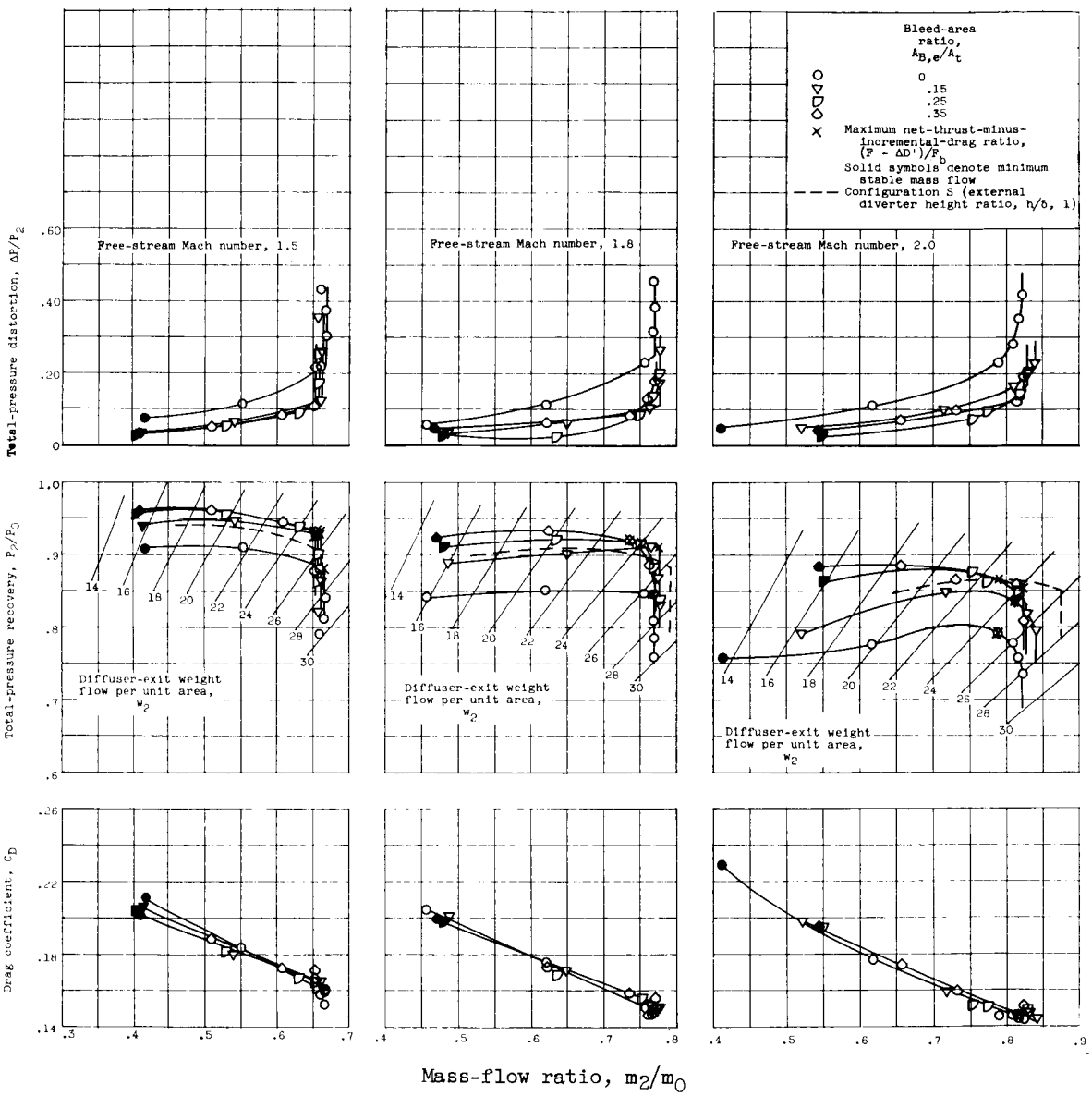

(k) Configuration P (perforated-ramp inlet without side fairings). External diverter height ratio, 1.

Figure 4. - Continued. Performance characteristics of inlet configurations.

[redacted]

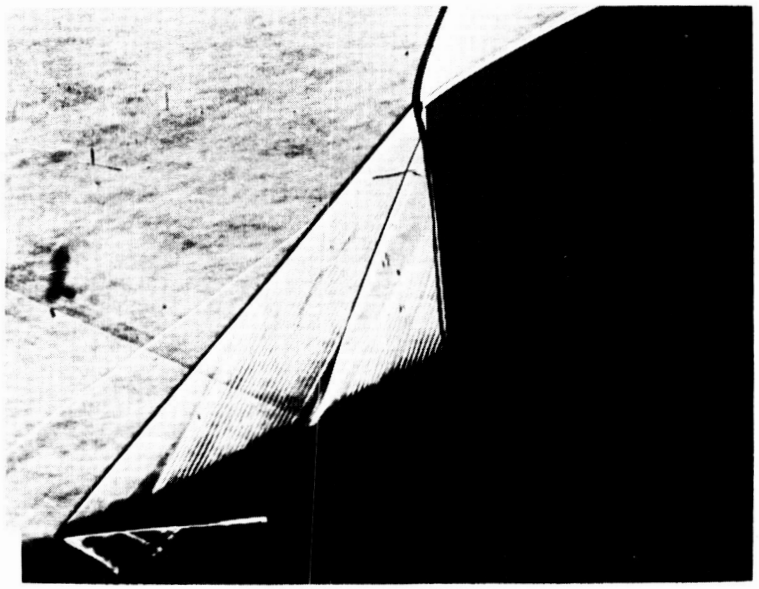

Approximately critical; mass-flow ratio, 0.82; total-pressure recovery, 0.85

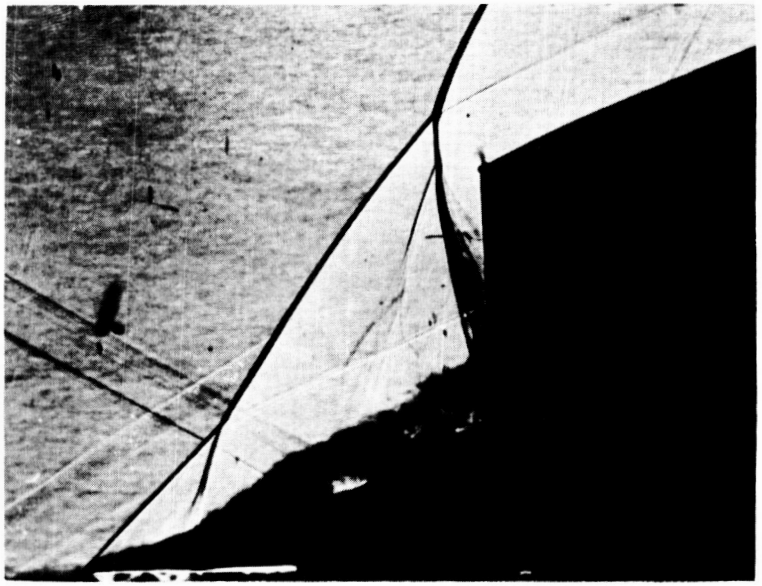

Subcritical; mass-flow ratio, 0.55; total-pressure recovery, 0.86 (minimum stable)

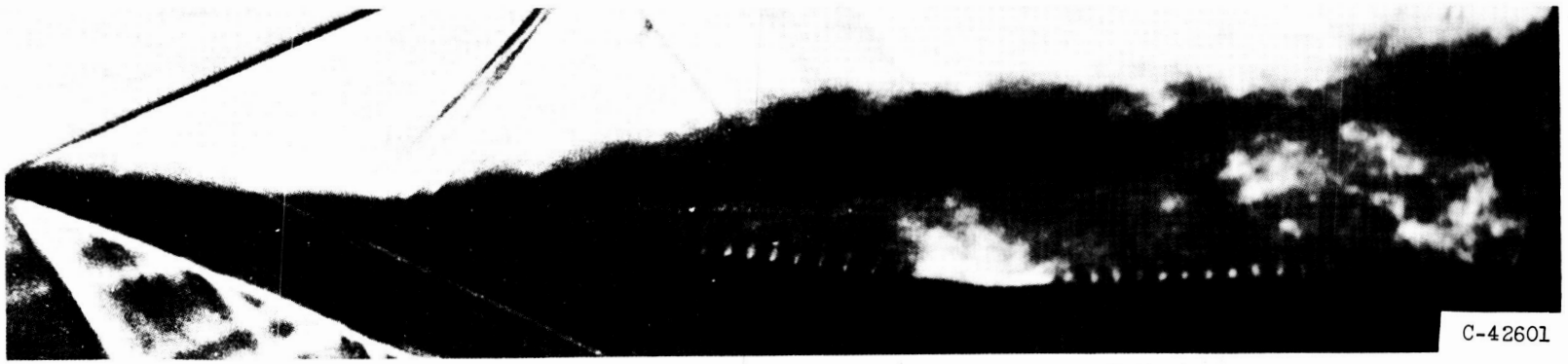

Enlarged view of ramp for subcritical mass flow

(l) Schlieren photographs of configuration P (perforated-ramp inlet without side fairings) at Mach number 2.0. Bleed-area ratio, 0.25; external diverter height ratio, 1.

Figure 4. - Concluded. Performance characteristics of inlet configurations.

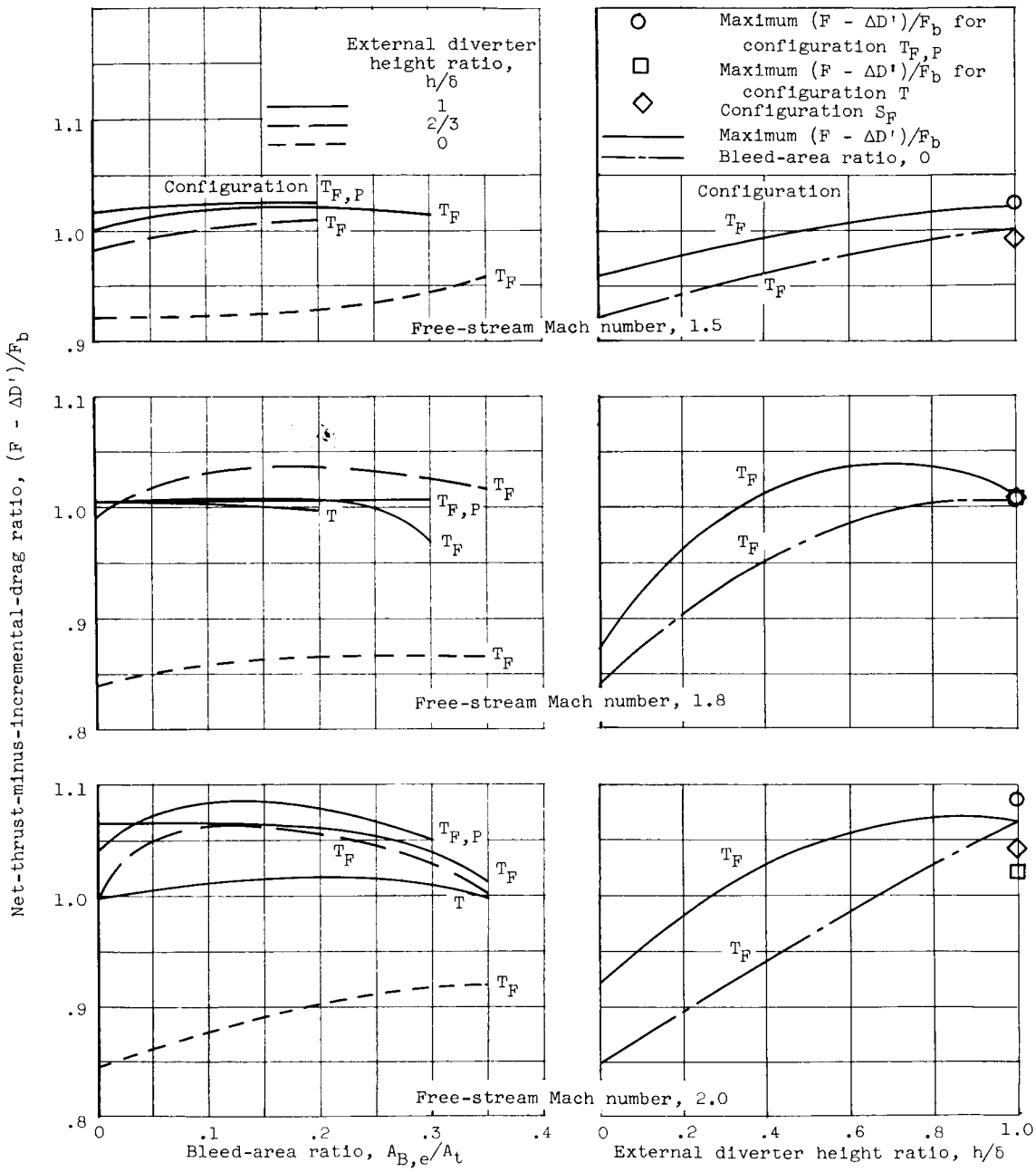

(a) Throat-bleed inlet.

Figure 5. - Effect of bleed and diverter height on net-thrust-minus-incremental-drag ratio.

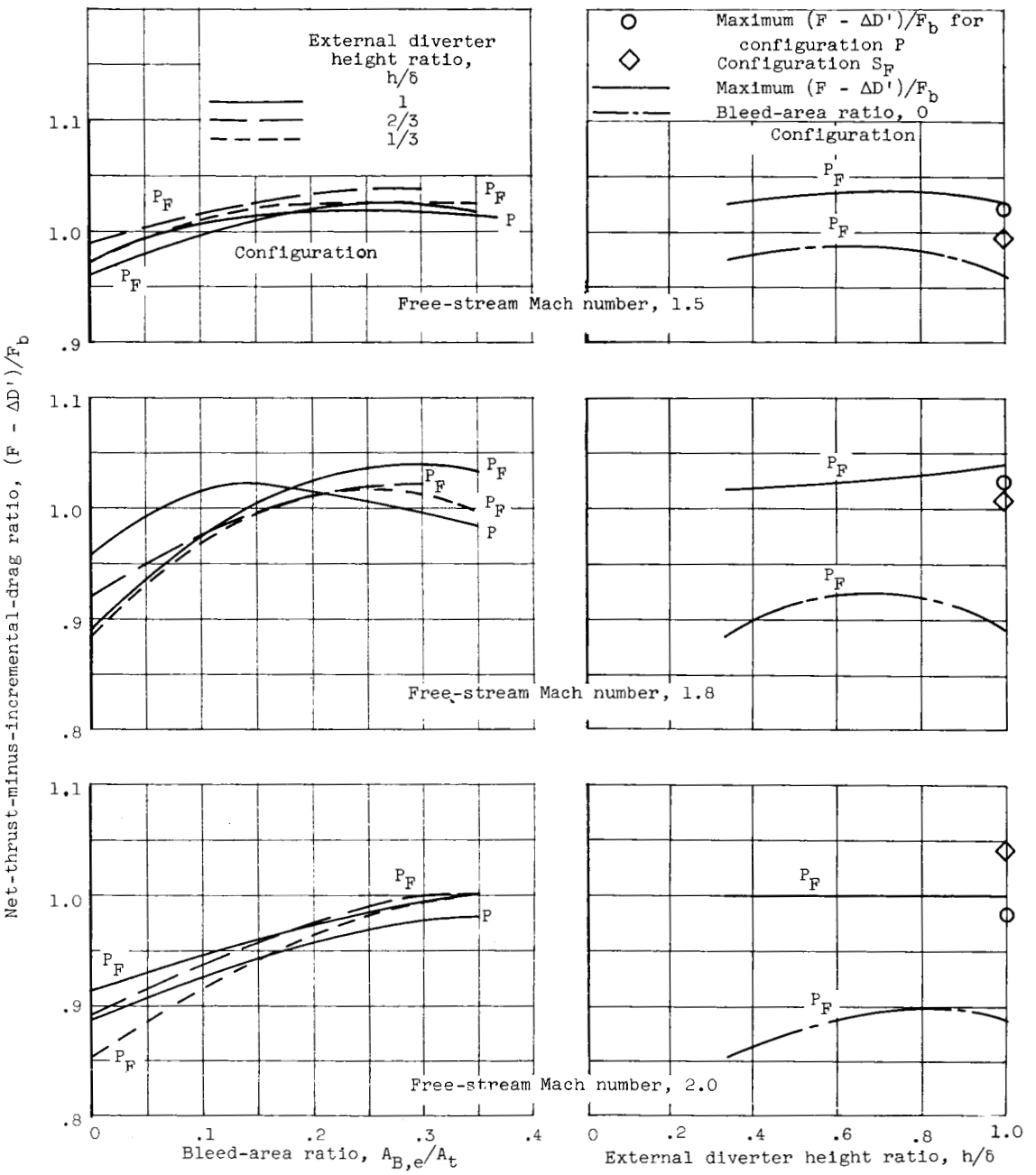

(b) Perforated-ramp inlet.

Figure 5. - Concluded. Effect of bleed and diverter height on net-thrust-minus-incremental-drag ratio.

Configuration	Free-stream Mach number					
	1.5		1.8		2.0	
	External diverter height ratio, h/δ	Bleed-area ratio, $A_{B,e}/A_t$	External diverter height ratio, h/δ	Bleed-area ratio, $A_{B,e}/A_t$	External diverter height ratio, h/δ	Bleed-area ratio, $A_{B,e}/A_t$
S	1	----	1	----	1	----
S_F	1	----	1	----	1	----
T_F	1	0.1	2/3	0.2	1	0.15
T	---	----	1	0	1	.2
$T_{F,P}$	1	.2	1	.25	1	.1
P_F	2/3	.3	1	.25	1	.35
P	1	.25	1	.15	1	.35
Ref. 4	1/3	.18	1/3	.18	1	.13

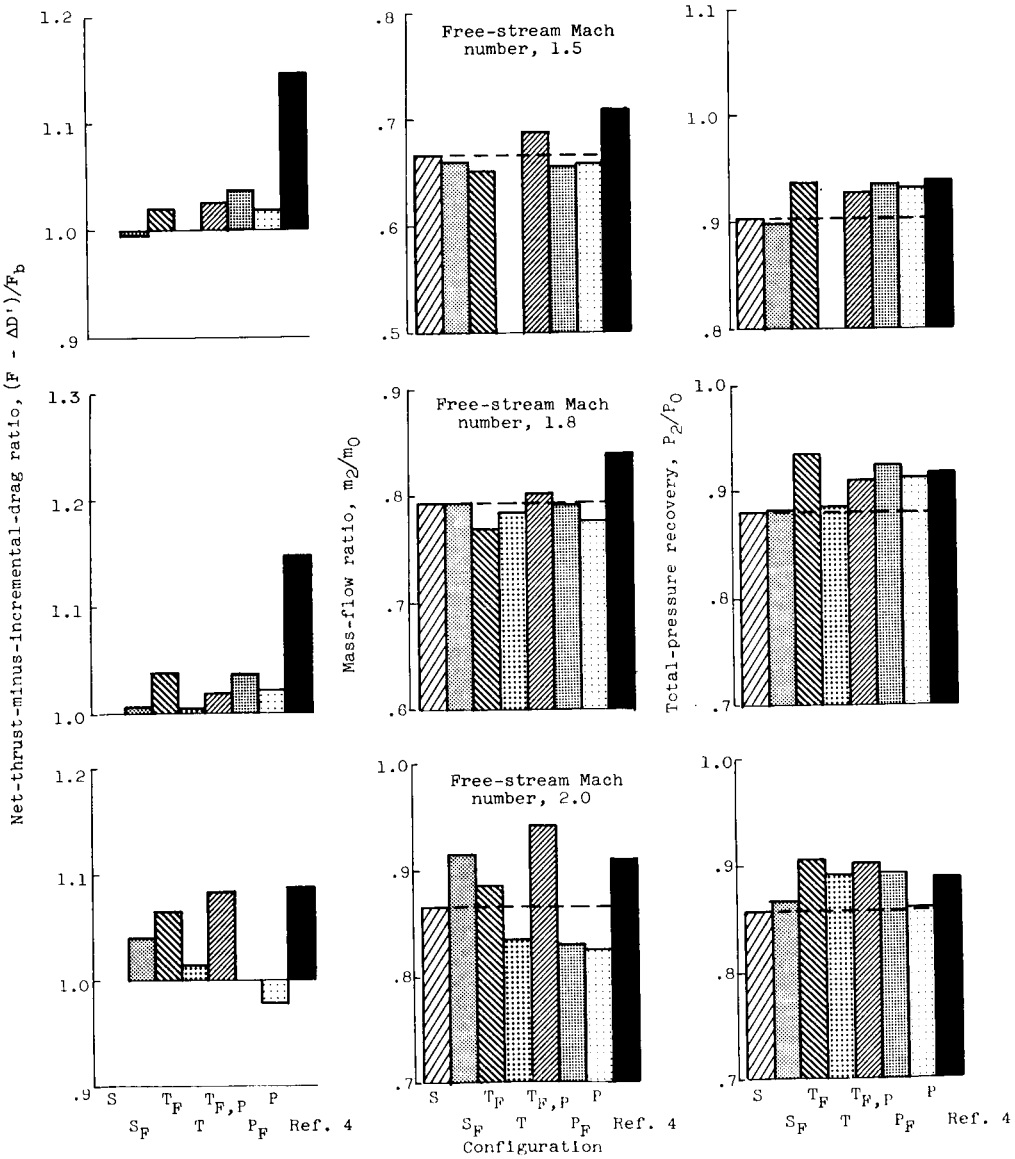

Figure 6. - Maximum net-thrust-minus-incremental-drag ratios and corresponding inlet performance.

Configuration	Free-stream Mach number					
	1.5		1.8		2.0	
	External diverter height ratio, h/δ	Bleed-area ratio, $A_{B,e}/A_t$	External diverter height ratio, h/δ	Bleed-area ratio, $A_{B,e}/A_t$	External diverter height ratio, h/δ	Bleed-area ratio, $A_{B,e}/A_t$
S	1	----	1	----	1	----
S_F	1	----	1	----	1	----
T_F	1	0.1	2/3	0.2	1	0.15
T	---	----	1	0	1	.2
$T_{F,P}$	1	.2	1	.25	1	.1
P_F	2/3	.3	1	.25	1	.35
P	1	.25	1	.15	1	.35
Ref. 4	1/3	.18	1/3	.18	1	.13

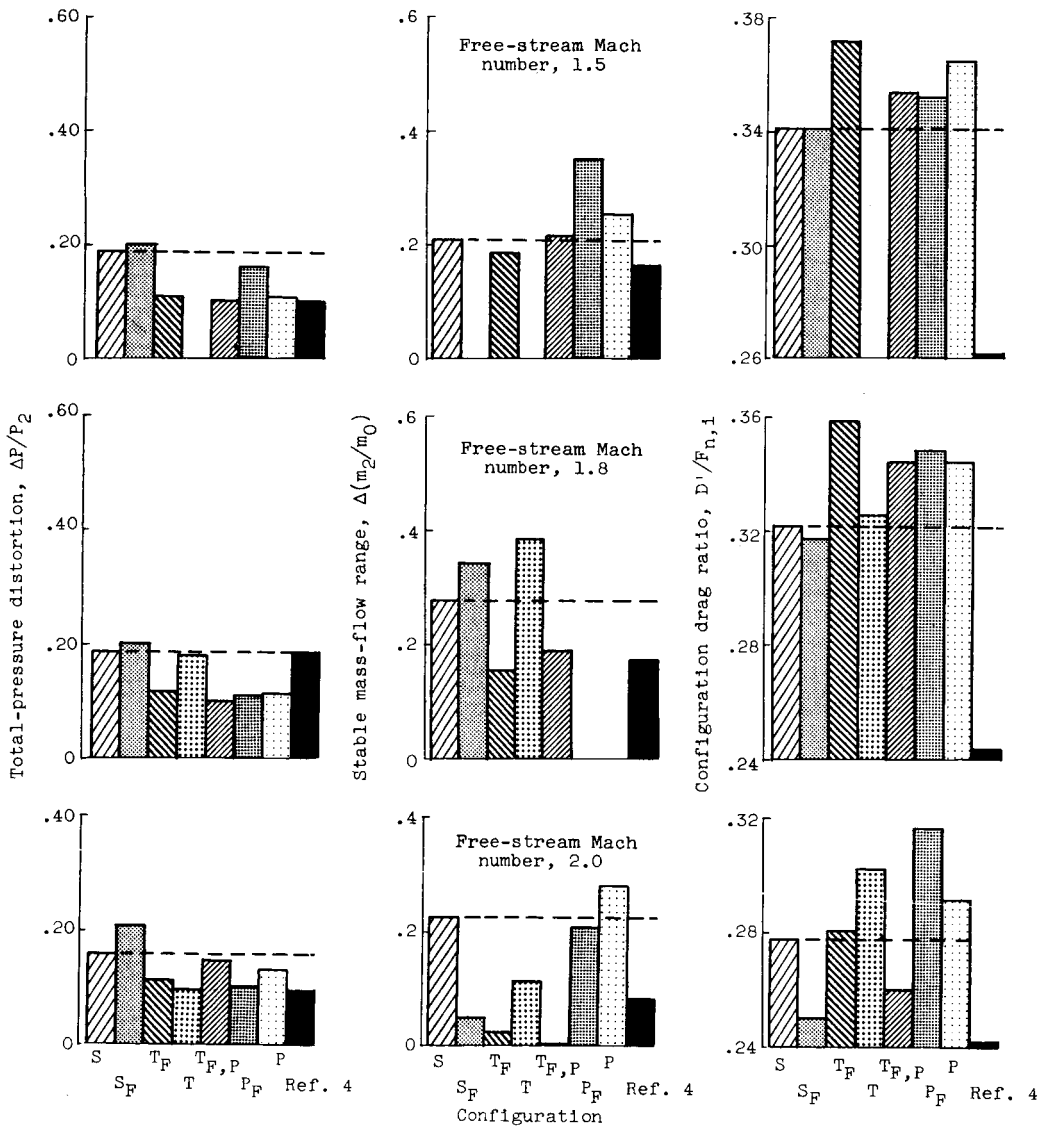

Figure 6. - Concluded. Maximum net-thrust-minus-incremental-drag ratios and corresponding inlet performance.